THE DESIGN OF THE FAST RASTER SYSTEM FOR THE EUROPEAN SPALLATION SOURCE

H.D. Thomsen*, S.P. Møller, ISA, Aarhus University, 8000 Aarhus C, Denmark

Abstract

The European Spallation Source (ESS) will nominally operate with an average (peak) proton current of 2.5 mA (62.5 mA) at 2.0 GeV. To reduce the beam peak current density at the spallation target, the ESS High Energy Beam Transport (HEBT) will apply a fast transverse raster system consisting of 8 dithering magnet dipoles. The raster system sweeps the linac beamlet on the target surface and gives a rectangular intensity outline within a macropulse of 2.86 ms. The magnets are driven by triangular current waveforms of up to 40 kHz. The preliminary magnet design and power supply topology will be discussed.

INTRODUCTION

As mentioned in [1, 2], the ESS will apply a raster system that sweeps the accelerator beamlet centroid in a transverse pattern on the target surface. By generating an effective, time-averaged distribution on the target, the solution should in general lower the time-averaged beam intensity and match a rectangular footprint of 180×60 mm^2 (H×V).

A Lissajous-like pattern is chosen to generate a 2D mesh of interweaved sweep trajectories. The pattern is defined by a frequency ratio f_x/f_y and phase ϕ_{xy} of two non-harmonic sweep waveforms in the transverse planes. Choosing very non-harmonic frequencies, e.g. $f_y/f_x = 113/83$, the patterns can reach almost limitless complexity, vastly exceeding that of a traditional raster pattern. If the raster frequencies f_w ($w = x, y$) can be defined as $f_w = n_w/T_0$ with n_w being integers, the raster pattern is closed with a period of T_0. The pattern features $n_x \times n_y$ lobes where n_x/n_y is a irreducible fraction. The resulting sweep pattern will of course be convoluted with the beam profile. The uniformity of the resulting distribution will depend on the spacing between the respective sweeps relative to the beamlet size. A fine mesh (large $n_x \times n_y$) would also to a large extent smear the beam profile, thus leaving the effective distribution more insensitive to the details of the beamlet profile. Similar systems have been considered for other high-power accelerators [3, 4].

The total raster system is foreseen to consist of $n_{RSM} = 8$ subsystems: 8 colinear raster scanning magnets (RSMs), two sets of 4 acting in the respective transverse planes. The RSMs in a set should ideally be synchronized and share the same field amplitude. Each RSM is, however, powered by a dedicated modulator. Not only does this modular design reduce the magnetic load on the RSMs and the peak output power of each modulator, but it is also a straightforward approach to implement redundancy and in general reduce

---

* heinetho@phys.au.dk

Table 1: Top Level Parameters and Specifications of a RSM

Parameter	Unit	Value
Beam rigidity	T.m	9.29
Beam pulse (4%)	ms	2.86
Raster pulse (5%)	ms	3.57
Max. f_w	kHz	40
Waveform	—	Triangle
Min. magnet aperture	mm	100
Magnetic length	mm	300
Turns per coil	—	2
Peak strength	mT.m	5
Nom. strength (H / V)	mT.m	1.6 / 2.3
Nom. deflection (H / V)	mrad	0.17 / 0.25
Max. current (peak-to-peak)	A	±340
Max. voltage (peak-to-peak)	V	±650

the impact of element failures. The total system is specified to be able to deliver nominal operation, despite a single permanent RSM or modulator failure in each set. The remaining 3 RSM subsystems (RSM + modulator) in the set can then be adjusted to compensate with 33% amplitude increase. Each subsystem thus provides a notable contingency in the available peak bending strength, cf. Table 1. Similarly, an increased beam rigidity, in case of linac upgrades, can be compensated by simply adding more raster units.

To avoid the need for active cooling of magnets and power supplies, the raster system is foreseen to be operated at a duty cycle of only 5%, appropriately more than the 4% beam pulse duty cycle, 2.86 ms at 14 Hz. The duty cycle of the pulsed RSM system is dictated by an external gate signal synchronized with the beam pulses.

RASTER MAGNET

A cross section and side view of a horizontal RSM (*i.e.* with a vertical field component) can be seen in Fig. 1. The magnet is based on a window frame yoke that gives good field uniformity in a large region of the magnet aperture. To avoid burn-in near pattern edges and corners, the sweep speeds should ideally be constant, while the direction alternates as dictated by the frequency. The magnet field should thus follow a triangle waveform. The considerable operating frequency—including the harmonics necessary for the triangle waveform—calls for materials with low Eddy current losses and a high frequency response. A NiZn ferrite yoke, possibly CMD5005 from Ceramic Magnetics, would be an obvious choice. Due to the skin depth in Cu, $\delta = 0.3$ mm $\times \sqrt{40 \text{ kHz}/f_w}$, the magnet coils will not bene-
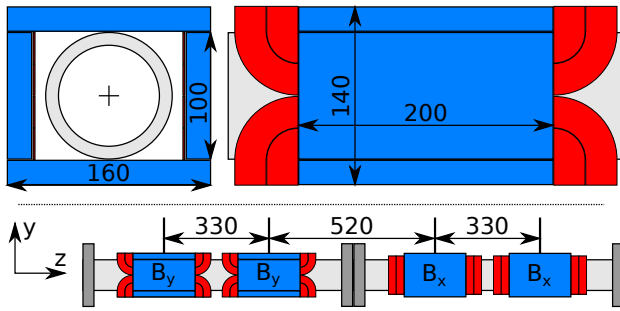
Figure 1: Dimensions of a raster magnet (top panel) and the positioning of RSM pairs introducing orthogonal field components (bottom panel). Ferrite parts are shown in blue and copper coils are shown in red. An outer frame to hold the yoke pieces together is not shown here.

fit from bulk volume being more than $\simeq 0.5$ mm from the coil surface. The conductors are thus cut from a 1 mm thick OFHC Cu plate and bent into 2-turn bedstead coils, cf. Fig. 1. Additionally, the vacuum chamber needs to be ceramic, possibly with an inner $\simeq 1$ μm Ti layer to conduct beam image currents and avoid heating of the ferrite yoke. If applied, care should be taken to the thickness of the metallization, such that it does not excessively affect the field waveform. It is worth stressing that introducing a constant delay in field is not considered critical if similar in all magnets, whereas attenuation of the field amplitude will have to be compensated by increasing the modulator amplitude setpoint. The same RSM design is applicable to both the horizontal and vertical family of RSMs, differing only by orientation. The RSMs are placed in pairs of identical field direction, $(B_y B_y)(B_x B_x)(B_x B_x)(B_y B_y)$. A RSM pair shares a single 850 mm ceramic vacuum tube with metallic flange connections, and the first half of the raster system is shown in the lower panel of Fig. 1.

RASTER MAGNET POWER SUPPLY

Each raster power supply is based on an input and output converter with appropriate controls and diagnostics. The input converter is designed as a capacitor charging DC unipolar power supply. The steady voltage V_0 at the DC link is then modulated by a IGBT-based H-bridge inverter. The 4 high-power IGBTs (SWA–SWD) in each modulator are switched in pairs (SWA+SWC & SWB+SWD) as dictated by a reference switching clock of $2f_w$. Flyback diodes are added in antiparallel to each IGBT to protect the switch against flyback spikes.

Figure 2 shows a sketch of the signals in a raster subsystem (HV power supply + modulator + RSM). For a purely inductive load (L_l), the produced square magnet voltage waveform, $V_l(t)$, will result in a triangle current waveform. It should be noted that since V_l (*i.e.* V_0) and the total inductance determines the constant magnet current slope, $\dot{I} = V_l/L_l$, the current amplitude of the triangle waveform will depend also on the switching times, *i.e.* f_w. The induced magnet current is thus produced by simply relying on dy-
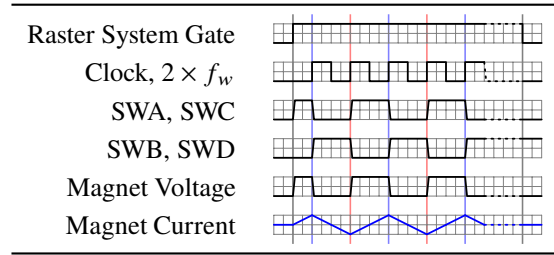
04 Hadron Accelerators

A14 Neutron Spallation Facilities

Figure 2: A sketched timing diagram of a RSM unit.

Table 2: Electrical Parameters of RSM and Cables

Parameter	Unit	RSM	Cable
Resistance	mΩ	2.1	41
Inductance	μH	6.6	5.7
Capacitance	nF	—	17

namic electrical laws between the switching times. It is important to stress that whereas this modulator effectively generates the required triangle waveform, the RSMs will not be able to idle at specific deflections.

Cables

With the relatively large operating frequencies, a detailed inductance budget is crucial to guarantee performance. To avoid beam-induced damage and faults to sensitive electronics (*e.g.* the IGBTs), a separate modulator building will house the raster power supplies. This demands rather long cables, 30 m cable length between each modulator and RSM. At this scale, the cable inductance can easily exceed that of a RSM. Also, the skin and proximity effect need to be considered when choosing the cables. Litz wires are an obvious cable type candidate, considering the frequency. Long Litz wires are however believed to be difficult to obtain unless produced specifically for the RSM system. The current design is hence based on two readily available, cheap four core wires in parallel. The electrical parameters of the modelled RSM and cable are shown in Table 2. Cable optimization, the possibility of using more specialized cables, bundling, and other transient cable effects are topics for a more detailed study.

CONTROLS & REGULATION

In Fig. 3, a rough block diagram of the RSM system is presented. The control system should set the voltage of the DC supplies determining the DC link and thus the RSM waveform amplitude for fixed frequencies. Ideally, the array $V_0[n_{\text{RSM}}]$ will only contain two different values, one per plane. As mentioned, the timing system should provide a gate signal that determines the duty cycle of the RSM system relative to the beam timing reference. A master clock, maybe the ESS timing system's 10 MHz oven-controlled crystal oscillator (OCXO) locked to a stable frequency reference, is used to phase-lock the RSMs. Embedded in each modulator, a FPGA, or possibly a Direct Digital Synthesizer
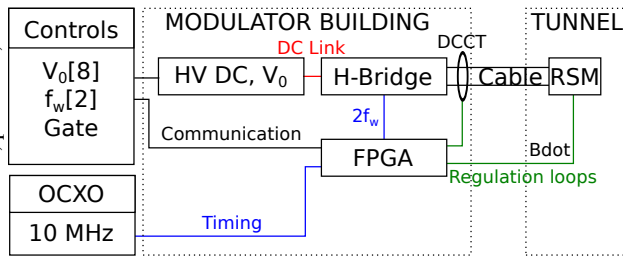
Figure 3: A block diagram of a single RSM subsystem. The DC link between the capacitor charged by a HV DC supply and the H-bridge modulator is marked with a red line.

(DDS), will also use this master clock to generate the $2f_w$ switch clock for the H-bridge.

Due to the large waveform frequency and principle of modulation, regulation on the fly during the 3.57 ms raster pulse is very difficult. Instead a slower regulation (pulse-to-pulse) will be implemented and maintained by a FPGA in each modulator. To regulate the waveform amplitude (*i.e.* the DC link voltages), each RSM will contain an inductive $\dot{B}$-loop. A feed-forward loop can use the resulting square voltage waveform amplitudes to adjust the DC link setpoint for the consecutive pulses. A DC offset in the current waveform can build up if a delay in the switching clock should occur. Such an offset can be detected by the integrated signals from DC current transformers measuring at the cables between each modulator and RSM. Again, the FPGA will regulate the DC offset over the next few pulses.

SYNCHRONIZATION

Substandard synchronization will degrade the pattern and the resulting beam distribution. There are three levels of synchronization that need to be addressed to ensure proper performance: within each raster modulator, magnet-to-magnet synchronization in a set, and finally maintaining the frequency ratio and phase ϕ_{xy} between the two planes. The first two sources will contribute to the upper cutoff frequency of the waveforms, whereas the latter could affect the generated pattern directly. The raster system should apply triangle waveforms, defined by an infinite sum of odd harmonics, with a corresponding ideal square waveform sweep velocity. Both waveforms will however be truncated by a finite bandwidth of the raster system, leading to finite rise and fall times (t_r) of the velocity waveform. To evaluate the necessary upper 3 dB cutoff frequency of the system ($f_{c,2}$), we compare the velocity waveform rise time $t_r \simeq 0.350/f_{c,2}$ with the time to sweep the beamlet 3 RMS sizes, $t_{3\sigma} = 3\sigma_w/4a_w f_w \simeq 1.9\ \mu$s, assuming the constant sweep speed far from the transition

$$\frac{t_{3\sigma}}{t_r} = \frac{f_{c,2}}{0.350}\frac{3\sigma_w}{4a_w f_w} = \frac{15}{7}\frac{\sigma_w}{a_w}\frac{f_{c,2}}{f_w}.$$

Ideally, $t_{3\sigma}/t_r \gg 1$, resulting in edges with an intensity not significantly larger than in the center of the distribution. The relative beamlet size thus compensates for a finite bandwidth of the raster system. Since $\sigma_w/a_w \gtrsim 0.1$, $f_{c,2} \gtrsim 5f_w = 200$ kHz is found.

Within each RSM modulator, the H-bridge IGBT switching time is believed to be the major contributor to $f_{c,2}$. Being of the order of $t_r \simeq 0.250\ \mu$s, this source is, however, almost an order of magnitude below $0.350/f_{c,2} = 1.75\ \mu$s and should thus be negligible.

Looking at each transverse plane, applying 4 colinear RSMs has many design and safety benefits but also introduces the challenge of maintaining magnet-to-magnet synchronization. While on average not affecting the combined deflection waveform in the regions far from the peaks, a phase distribution between the ideal RSM waveforms will reduce the sharpness of the peaks, thus reducing the effective cutoff frequency of the system. The synchronization of the n_{RSM} is believed to be possible better than 200 ns, again far below the bandwidth time scale.

With the example ratio $f_y/f_x = 113/83$, numerous raster patterns have been simulated for a wide range of waveform phases ϕ_{xy}. If anything, the dephasing $\phi_{xy} \neq 0$ appears to only improve the pattern complexity. For this pattern ratio, there does not appear to be a risk that a dephasing between the two planes could hit a lower pattern order and affect the beam intensity distribution uniformity.

CONCLUSION

The design of a fast raster system for the ESS has been presented. Based on low-inductance ferrite magnets and H-bridge modulators, the system is set to induce triangle waveform displacement modulations at the spallation target. The system is essential in meeting the facility's performance goals, hence stability and availability should be considered even early in the design phase. Likewise, a RSM subsystem is to be prototyped early.

From a preliminary assessment of the system concept, including transient circuit simulations, the design appears feasible and relatively inexpensive. More detailed studies are to be conducted by the end of 2014. We acknowledge valuable input to the system design from Tom Shea, Carlos Martins, Frithiof Jensen (ESS) and Niels Hauge, Franz Bødker, Alexander Elkiær (Danfysik A/S).

REFERENCES

[1] H.D. Thomsen *et al.*, IPAC'13, MOPEA005, p. 70 (2013).

[2] H.D. Thomsen *et al.*, IPAC'14, WEPRO073 (2014).

[3] S. Chapelle *et al.*, LINAC'98, TU4089, p. 612 (1998).

[4] B. Blind *et al.*, LINAC 2006, MOP055, p. 171 (2006).